JOURNAL OF THE ROYAL SOCIETY Interface

*J. R. Soc. Interface* (2009) **6**, 293–306
doi:10.1098/rsif.2008.0254
*Published online* 22 July 2008

# Complementary vasoactivity and matrix remodelling in arterial adaptations to altered flow and pressure

**A. Valentín[1], L. Cardamone[2], S. Baek[3] and J. D. Humphrey[1,*]**

[1]*Department of Biomedical Engineering, 337 Zachry Engineering Center, 3120 TAMU, Texas A&M University, College Station, TX 77843-3120, USA*
[2]*Dipartimento di Ingegneria Civile, Università degli Studi di Salerno, 84084 Fisciano, Italy*
[3]*Department of Mechanical Engineering, Michigan State University, East Lansing, MI 48824, USA*

Arteries exhibit a remarkable ability to adapt to sustained alterations in biomechanical loading, probably via mechanisms that are similarly involved in many arterial pathologies and responses to treatment. Of particular note, diverse data suggest that cell and matrix turnover within vasoaltered states enables arteries to adapt to sustained changes in blood flow and pressure. The goal herein is to show explicitly how altered smooth muscle contractility and matrix growth and remodelling work together to adapt the geometry, structure, stiffness and function of a representative basilar artery. Towards this end, we employ a continuum theory of constrained mixtures to model evolving changes in the wall, which depend on both wall shear stress-induced changes in vasoactive molecules (which alter smooth muscle proliferation and synthesis of matrix) and intramural stress-induced changes in growth factors (which alter cell and matrix turnover). Simulations show, for example, that such considerations help explain the different rates of experimentally observed adaptations to increased versus decreased flows as well as differences in rates of change in response to increased flows or pressures.

**Keywords: vascular growth; remodelling; smooth muscle mechanics; collagen deposition; stress**

## 1. INTRODUCTION

With considerable foresight, Rodbard (1975, p. 12) wrote:

> Let us assume that each endothelial cell is equipped with receptors which are sensitive to the magnitude of the drag force that impinges on it… Deviations of drag from this set-point initiate negative feedback mechanisms that return the magnitude of the drag to its set-point. In blood vessels, these effects appear to operate through two related mechanisms: an immediate physiological adjustment in vascular tone induced by the change in flow, and a delayed anatomical change that develops when the changed flow rate persists.

Although this scenario is most apparent in arterial adaptations to sustained alterations in blood flow, smooth muscle vasoactivity appears to play similar roles in cases of altered blood pressure and axial stretch as well as in diseases ranging from pulmonary hypertension to cerebral vasospasm. That is, diverse clinical observations and laboratory experiments over the past three decades (cf. Humphrey 2002) have confirmed Rodbard's general concept: many adaptations occur via matrix remodelling (i.e. delayed anatomical changes) within altered vasoactive states (i.e. adjustments in vascular tone) so as to maintain constant various mechanical factors. For a recent lucid review of the coupling between vasoactivity and matrix remodelling, see Dajnowiec & Langille (2007).

Prior computational models of the biomechanics of arterial adaptations have been based primarily on either the concept of kinematic growth (e.g. Taber 1998; Rachev 2000) or a constrained mixture theory (e.g. Gleason & Humphrey 2004; Gleason *et al.* 2004). The goal of this paper is to illustrate the importance of matrix remodelling within altered vasoactive states for basilar arteries in response to sustained alterations in blood flow and blood pressure. Towards this end, we employ an extended constrained mixture model of the arterial wall whereby the mass fractions, material properties and natural configurations of individual constituents can evolve separately and thereby dictate overall growth and remodelling (G&R).

## 2. METHODS

### 2.1. Wall mechanics and haemodynamics

We restrict our attention to elastostatics (cf. Humphrey & Na 2002) and two-dimensional wall mechanics (cf. Gleason *et al.* 2004), which can capture salient features of the structural stiffness and overall geometry

*Author for correspondence (jhumphrey@tamu.edu).

*Received* 11 June 2008
*Accepted* 25 June 2008

sufficient for many clinical and fluid–solid interaction studies (Humphrey & Taylor 2008). Hence, note that two-dimensional equilibrium equations for a straight, cylindrical segment of an artery can be written, at each G&R time $s$, as

$$\sigma_\theta(s) = \frac{P(s)a(s)}{h(s)}, \tag{2.1}$$

$$\sigma_z(s) = \frac{f(s)}{\pi h(s)(2a(s)+h(s))}, \tag{2.2}$$

where $P$ is the transmural pressure; $a$ is the deformed luminal radius; $h$ is the deformed wall thickness; and $f$ is the applied axial force. (Note that although often derived for thin-walled tubes, these mean values of stress also hold for thick-walled tubes exhibiting linear or nonlinear material behaviour and subjected to negligible perivascular tethering; Humphrey & Delange 2004.) The values of $a/h$ tend to be 7–10 in normal large arteries, thus yielding homeostatic values of circumferential stress of the order of 90–130 kPa at mean arterial pressure, which appear to be similar to computed values of axial stress (Humphrey & Wilson 2003).

Inasmuch as these two equilibrium equations are not sufficient to determine the three primary geometric variables for the wall (radius $a$, thickness $h$ and length $l$), even after introducing constitutive relations for the stress responses, we invoke a constancy of total mass density (Humphrey & Rajagopal 2002) to close this system of equations. That is, given that the mass density of the arterial wall $\rho(s) \cong \rho(0)$, let

$$\beta(s) = \frac{\pi h(s)(2a(s)+h(s))l(s)}{\pi h(0)(2a(0)+h(0))l(0)} \quad \forall\ s, \tag{2.3}$$

where $l$ denotes the deformed length of the segment and $\beta(s)$ describes overall changes in mass or volume, which are potentially measurable. It is assumed, of course, that all geometric values are known at G&R time $s=0$, where $\beta(0) \equiv 1$. Letting $l(s) \equiv l(0)$ allows us to solve for $a(s)$ or $h(s)$ at any G&R time $s$; marked increases in $l(s)$ can result in tortuous arteries, an important consideration in some cases (Lehman *et al.* 1991), but this complicates the biomechanics considerably.

Among others, Rodbard (1975) and Zamir (1977) recognized that Murray's (1926) result could be interpreted as a 'constancy of wall shear stress' if the mean wall shear stress is given by the solution of a steady, fully developed, laminar, one-dimensional, incompressible flow of a Newtonian fluid within a rigid circular tube (a rough approximation for an artery): $\tau_w = 4\mu Q/\pi a^3$, where $\mu$ is the viscosity of blood at high shear rates (approx. 3.5 cP); $Q$ is the volumetric flow rate; and $a$ is again the deformed luminal radius. That is, if $a^3$ remains proportional to $Q$ for a fixed viscosity, as suggested by Murray's simple analysis, then $\tau_w$ must remain constant.

### 2.2. G&R framework

We employ an extension (Baek *et al.* 2006) of a constrained mixture theory of isothermal G&R for soft tissues (Humphrey & Rajagopal 2002). The Cauchy stress response by the arterial wall $\boldsymbol{\sigma}$ results from passive elasticity and smooth muscle activation, and thus can be approximated as

$$\boldsymbol{\sigma} = \frac{1}{\det \boldsymbol{F}} \boldsymbol{F} \frac{\partial W}{\partial \boldsymbol{F}^{\mathrm{T}}} + \sigma_\theta^{\mathrm{act}}(\mathrm{Ca}^{++}) \boldsymbol{e}_\theta \otimes \boldsymbol{e}_\theta, \tag{2.4}$$

where $\boldsymbol{F}$ is the deformation gradient; $W$ is a stored energy function for the elastic response; and $\sigma_\theta^{\mathrm{act}}$ denotes the smooth muscle contractility that exists primarily in the circumferential direction and ultimately depends on intracellular calcium. Herein, we restrict our attention to $\boldsymbol{F} = \mathrm{diag}[\lambda_z, \lambda_\theta]$. By the rule of mixtures, the stored energy can be thought of conceptually as $W = \sum \phi^k W^k$, where $\phi^k = \rho^k/\rho$ are constituent mass fractions. Assuming that G&R commences at $s=0$, Baek *et al.* (2006) proposed the following relations for the evolving constituent mass densities and strain energy functions:[1]

$$M^k(s) = M^k(0) Q^k(s) + \int_0^s m^k(\tau) q^k(s,\tau) \mathrm{d}\tau, \tag{2.5}$$

$$W^k(s) = \frac{M^k(0)}{\rho(s)} Q^k(s) \widehat{W}^k\left(\boldsymbol{C}^k_{n(0)}(s)\right) + \int_0^s \frac{m^k(\tau)}{\rho(s)} q^k(s,\tau) \widehat{W}^k\left(\boldsymbol{C}^k_{n(\tau)}(s)\right) \mathrm{d}\tau, \tag{2.6}$$

where $Q^k(s) \in [0,1]$ account for fractions of material produced at or before time $s=0$ that survive to time $s$, with $Q^k(0) \equiv 1$; $m^k(\tau) \geq 0$ are true mass density production rate functions; and $q^k(s,\tau) \in [0,1]$ account for the fractions of material produced at time $\tau \in [0,s]$ that survive to time $s$. Moreover, $M^k(s)$ is the mass per unit area of constituent $k$ at time $s$ and $\widehat{W}^k$ is the energy stored elastically in constituent $k$, which depends on $\boldsymbol{C}^k_n$, the right Cauchy–Green tensor for that constituent defined relative to its individual natural configuration. In particular, $\boldsymbol{C}^k_{n(\tau)}(s) = (\boldsymbol{F}^k_{n(\tau)}(s))^{\mathrm{T}} \boldsymbol{F}^k_{n(\tau)}(s)$, where $\boldsymbol{F}^k_{n(\tau)}(s) = \partial \boldsymbol{x}^k(s)/\partial \boldsymbol{X}^k(\tau)$, with $\boldsymbol{x}^k(s) = \boldsymbol{x}(s)$ consistent with the concept of a constrained mixture and $\boldsymbol{X}^k(\tau)$ reflecting evolving natural configurations for constituent $k$ when produced at time $\tau$. Clearly, the survival functions $q^k(s,\tau)$ ensure that a constituent contributes to load bearing only until it is degraded, which owing to the convolution integral is reminiscent of a fading memory behaviour, characteristic of viscoelasticity, wherein a constituent contributes more to the stress response the more recently it was produced. Finally, note that $\sum \rho^k(s) = \sum \rho^k(0)$ is consistent with (2.3).

### 2.3. Specialization for two-dimensional wall mechanics

Combining the equilibrium equations and constitutive relations for the principal tensions $T_i = \sigma_i h$, where $i = z, \theta$, we have at any G&R time $s$

$$Pa = T_\theta = \frac{1}{\lambda_z} \sum \frac{\partial W^k}{\partial \lambda_\theta} + \sigma_\theta^{\mathrm{act}} h, \tag{2.7}$$

$$\frac{f}{\pi(2a+h)} = T_z = \frac{1}{\lambda_\theta} \sum \frac{\partial W^k}{\partial \lambda_z}. \tag{2.8}$$

[1]See appendix A for evaluations of special cases for these constitutive functions. Note that the original paper denoted G&R time via $t$ rather than $s$.

In general, for a fibrous constituent $k$ (e.g. collagen), we have

$$\frac{\partial \widehat{W}^k\left(\lambda^k_{n(\tau)}(s)\right)}{\partial \lambda_\theta(s)} = \frac{\partial \widehat{W}^k(s)}{\partial \lambda^k_{n(\tau)}}\frac{\partial \lambda^k_{n(\tau)}}{\partial \lambda_\theta(s)} = \frac{\partial \widehat{W}^k(s)}{\partial \lambda^k_{n(\tau)}}\frac{G^k_{\mathrm{h}}}{\lambda(\tau)}\frac{\partial \lambda(s)}{\partial \lambda_\theta(s)}, \tag{2.9}$$

$$\frac{\partial \widehat{W}^k\left(\lambda^k_{n(\tau)}(s)\right)}{\partial \lambda_z(s)} = \frac{\partial \widehat{W}^k(s)}{\partial \lambda^k_{n(\tau)}}\frac{\partial \lambda^k_{n(\tau)}}{\partial \lambda_z(s)} = \frac{\partial \widehat{W}^k(s)}{\partial \lambda^k_{n(\tau)}}\frac{G^k_{\mathrm{h}}}{\lambda(\tau)}\frac{\partial \lambda(s)}{\partial \lambda_z(s)}, \tag{2.10}$$

with $\lambda^k_{n(\tau)}(s) = G^k_{\mathrm{h}}(\lambda(s)/\lambda(\tau))$ and

$$\lambda(\tau) = \sqrt{\lambda_z^2(\tau)\cos^2\left(\alpha^k_0\right) + \lambda_\theta^2(\tau)\sin^2\left(\alpha^k_0\right)} \quad \forall\ \tau \in [0, s], \tag{2.11}$$

where $\alpha^k_0$ denotes the angle between a fibre and the $z$-axis in a common reference configuration for the mixture (i.e. artery). These kinematic relations are derived by Baek *et al.* (2006). Note that $G^k_{\mathrm{h}}$ represents a basic hypothesis in the theory, that new fibres are incorporated within extant tissue at a preferred (homeostatic) stretch. We call $G^k_{\mathrm{h}}$ the 'deposition stretch'. Finally, one must prescribe the direction in which the fibre is deposited. Without loss of generality, herein, we assume that fibre directions are preserved in the non-pathological cases of adaptations to altered flow and pressure.

### *2.4. Illustrative constitutive relations*

As revealed by the G&R framework, constitutive relations are needed for the true mass density productions, survival functions and stress responses for the individual structurally significant constituents (elastin, fibrillar collagen and smooth muscle) as well as for the deposition stretches and deposition alignment. Although there is need for much more research on the precise forms of each of these relations and best-fit values of the associated material parameters, the considerable data available in the literature enable one to postulate relations sufficient for illustrative purposes. Vascular elastin is typically assumed to be isotropic and to exhibit a neo-Hookean-type response (Dorrington & McCrum 1977; Holzapfel *et al.* 2000), hence we assume that the elastin-dominated amorphous matrix is described by

$$\widehat{W}^{\mathrm{e}}(s) = c\left(\lambda^{\mathrm{e}}_\theta(s)^2 + \lambda^{\mathrm{e}}_z(s)^2 + \frac{1}{\lambda^{\mathrm{e}}_\theta(s)^2\lambda^{\mathrm{e}}_z(s)^2} - 3\right), \tag{2.12}$$

where $c$ is a material parameter. Moreover, we assume that most of the elastin is produced in the perinatal period and that it is normally very stable biologically (Langille 1996; Stenmark & Mecham 1997). Hence, we assume that in non-pathological conditions $Q^{\mathrm{e}}(s) = 1$ and $m^{\mathrm{e}}(\tau) = 0 \ \ \forall \ \ s, \tau \in [0, \infty)$. Collagen and vascular smooth muscle, on the other hand, appear to turnover continuously but slowly in the normal arterial wall, albeit at different basal rates $m^k_0$. We assume that for each family of collagen and circumferentially oriented passive smooth muscle (Baek *et al.* 2006),

$$\widehat{W}^k(s) = c^k_1\left(\exp\left(c^k_2\left(\lambda^k_{n(\tau)}(s)^2 - 1\right)^2\right) - 1\right), \tag{2.13}$$

and for active smooth muscle (Rachev & Hayashi 1999),

$$\sigma^{\mathrm{act}}_\theta(s) = T_{\max}\phi^{\mathrm{m}}(s)\left(1 - \mathrm{e}^{-C(s)^2}\right) \times \lambda^{\mathrm{m(act)}}_\theta(s)\left[1 - \left(\frac{\lambda_{\mathrm{M}} - \lambda^{\mathrm{m(act)}}_\theta(s)}{\lambda_{\mathrm{M}} - \lambda_0}\right)^2\right], \tag{2.14}$$

where $T_{\max}$ is a scaling parameter with units of N m$^{-2}$; $\lambda_{\mathrm{M}}$ is the circumferential stretch at which the active stress is maximum; and $\lambda_0$ is the circumferential stretch at which the active stress goes to zero. $C(s)$ is the net ratio of constrictors to dilators and $\lambda^{\mathrm{m(act)}}_\theta(s) = a(s)/a^{\mathrm{m(act)}}(s)$, where $a^{\mathrm{m(act)}}(s)$ can evolve via a first-order rate equation (cf. Baek *et al.* 2007). For these simulations, we consider

$$C(s) = C_{\mathrm{B}} - C_{\mathrm{S}}\left(\frac{\tau_{\mathrm{w}}(s) - \tau^{\mathrm{h}}_{\mathrm{w}}}{\tau^{\mathrm{h}}_{\mathrm{w}}}\right), \tag{2.15}$$

where $C_{\mathrm{B}}$ is the basal constrictor to dilator ratio; $C_{\mathrm{S}}$ is a scaling factor for the shear-induced change in constrictor concentration; and $\tau_{\mathrm{w}}(s)$ and $\tau^{\mathrm{h}}_{\mathrm{w}}$ are the shear stress at G&R time $s$ and the homeostatic state, respectively. The instantaneous change in active stress as a function of stretch and constrictor concentration is shown in figure 1. Note that this active behaviour is taken with respect to individual unloaded configurations for smooth muscle (cf. fig. 1 in Baek *et al.* 2006), not for the entire mixture.

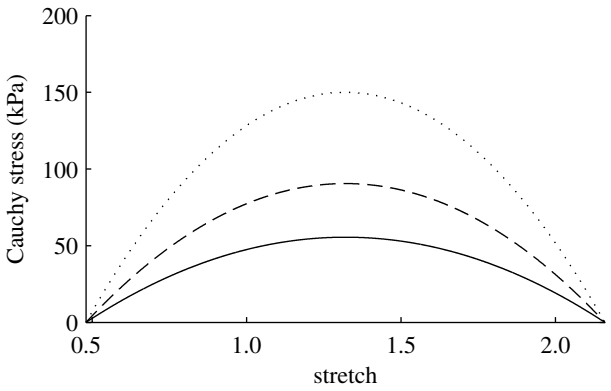


Figure 1. Active response by smooth muscle where $C = C_{\mathrm{B}}$ (solid curve), $2C_{\mathrm{B}}$ (dashed curve) and $\infty$ (dotted curve). Stretch is expressed with respect to the muscle's natural configuration. Increases in $C$ result in corresponding increases in active stress for a given stretch.

As in prior work (Taber 1998; Rachev 2000; Gleason *et al.* 2004; Baek *et al.* 2007), we let mass density production rates depend in part on differences in intramural stress from homeostatic values. In addition, however, we know that vasoactive molecules regulated by the endothelium in response to altered wall shear stress also affect cell and matrix turnover. For example, nitric oxide (NO) is an inhibitor of smooth muscle proliferation and synthesis of collagen (Rizvi & Myers

1997), whereas endothelin-1 (ET-1) is a promoter of smooth muscle proliferation and synthesis of collagen (Rizvi *et al.* 1996); NO is upregulated in response to increased wall shear stress and ET-1 is upregulated in response to decreased shear (Malek & Izumo 1992; Uematsu *et al.* 1995). Many other endothelially derived molecules (vasoactive, growth regulatory and proteases) are regulated similarly. In principle, then, $m^k = f^k(\sigma_\theta, \sigma_z, \tau_w)$ for $k$=collagen and smooth muscle. Alternatively, anticipating the future use of reaction–diffusion equations to determine concentration histories for diverse soluble substances, we can let $m^k = f^k(\sigma_\theta, \sigma_z, C)$, where $C$ is the aforementioned ratio of constrictors to dilators. Specifically, we consider the following candidate constitutive relation for true mass density productions:

$$m^k = m_0^k\big(1 + K_\sigma^k \Delta\sigma + K_C^k \Delta C\big), \tag{2.16}$$

where $m_0^k$ is the basal production rate; $K_j^k$ are 'rate parameters' that govern stress- and constrictor-mediated changes in production; and $\sigma$ is a scalar metric for wall stress as in Baek *et al.* (2007). In a three-dimensional model, $\sigma$ and $C$ would be field quantities, but we focus on mean values here. For example, mass density productions can be prescribed individually for fibre families based on the stress borne by that family. Moreover, $\Delta\sigma$ and $\Delta C$ represent normalized differences in stress or constrictors from their homeostatic values. Hence, in the case where these differences are zero, one recovers homeostatic production rates. Finally, although the kinetics of cell apoptosis and matrix degradation are extremely complex, it appears that gross responses follow first-order-type kinetics. Hence, let the survival functions

$$q^k(s,\tau) = \exp\left(-\int_\tau^s K^k(\tilde{\tau})\mathrm{d}\tilde{\tau}\right), \tag{2.17}$$

where the functions $K^k(\tilde{\tau})$ are rate-type parameters for mass removal having units of day$^{-1}$. Of course, the rates of removal can also depend explicitly on changes in the tension within fibres; hence one specific form to consider is

$$K^k(\tilde{\tau}) = K_h^k + K_h^k \Delta\zeta(\tilde{\tau})^2, \tag{2.18}$$

where $K_h^k$ is an initial value for the rate parameter; $\Delta\zeta(\tilde{\tau})$ is the difference in fibre tension from its homeostatic value; and $\zeta^{k(\tau)}$ is the level of tension on constituent $k$ that was produced at time $\tau$ and defined by

$$\zeta^{k(\tau)}(s) = \frac{\partial \widehat{W}^k/\partial\lambda_n^k\left(\lambda_{n(\tau)}^k(s)\right)}{\partial \widehat{W}^k/\partial\lambda_n^k\left(G_h^k\right)}. \tag{2.19}$$

In summary, our two primary governing equations are

$$Pa = T_\theta^e + \frac{1}{\lambda_z}\sum\frac{\partial W^j}{\partial\lambda_\theta} + \frac{1}{\lambda_z}\frac{\partial W^m}{\partial\lambda_\theta} + \sigma_\theta^{act}h \quad \forall\ s, \tag{2.20}$$

$$\frac{f}{\pi(2a+h)} = T_z^e + \frac{1}{\lambda_\theta}\sum\frac{\partial W^j}{\partial\lambda_z} \quad \forall\ s, \tag{2.21}$$

subject to the mass density constraint (equation (2.3)), where $T_i^e$ are tensions borne by elastin. Recall that superscripts 'm' and 'e' denote passive smooth muscle and unchanging elastin, respectively. Moreover, we allow $j$ families of collagen fibres, each defined by different parallel orientations. In particular, it appears that $j$=2 or 4 allows one to model the complex contributions of the collagen reasonably well (Holzapfel *et al.* 2000; Baek *et al.* 2007). We employ four families of collagen (cf. Wicker *et al.* 2008) for basilar arteries: axial, circumferential and two helical families with $\alpha_0^k = \pm 45°$.

## 3. ILLUSTRATIVE RESULTS

### 3.1. Altered flow

It is well accepted that sustained increases (or decreases) in blood flow result in an increased (or decreased) arterial calibre (Kamiya & Togawa 1980; Langille & O'Donnell 1986; Langille *et al.* 1989; Brownlee & Langille 1991; Rudic *et al.* 1998), often with increased (or decreased) thickening of the wall and possible changes in length (Zarins *et al.* 1987; Lehman *et al.* 1991).

A change in blood flow will have an almost immediate effect on vessel geometry due to smooth muscle relaxation or contraction in response to endothelial production of NO or ET-1, respectively. Of course, smooth muscle can only relax or contract within a certain range. If $\tau_w^h$ can be restored by an acute dilation or constriction within the active range of the smooth muscle, no further change in calibre will be observed. In the cases herein, the basilar artery is allowed to accommodate up to an approximately 3 per cent active dilation and an approximately 30 per cent active constriction. Figure 2 illustrates the consequences of altered muscle tone as a function of altered flow rate as well as the beginning of G&R as prescribed by the above dependencies of mass density production and the removal on changes in wall stress and constrictor concentration. The model captures the maximum dilation and constrictions inherent to smooth muscle due to the prescribed $\lambda_M$ and $\lambda_0$ (table 1).

If flow rate is altered beyond a certain threshold, however, the smooth muscle will not be able to restore $\tau_w^h$ by a single instantaneous change in diameter. Rather, a maximum instantaneous dilation or constriction will occur, to be followed by a more gradual convergence via G&R (see equations (2.15)–(2.18) and figures 3 and 4) to the calibre at which shear stress returns to normal. This two-step change in inner radius is due to reorganization and/or turnover of smooth muscle and collagen (see below) as new constituents are deposited at their homeostatic prestretches, thus allowing further dilation or constriction as needed (Gleason *et al.* 2004; Gleason & Humphrey 2005*a*,*b*; Baek *et al.* 2007).

For cases in which reductions in flow were beyond what the extant active muscle could accommodate, predictions suggested that inner radius could be stabilized within two weeks (figure 4). The model imposes no upper bound to constrictor concentrations, which in addition to changes in stress can drive substantial instantaneous constrictions and rapid subsequent G&R-driven changes. On the other hand, the lower bound limit of $C$=0 means that any G&R-driven

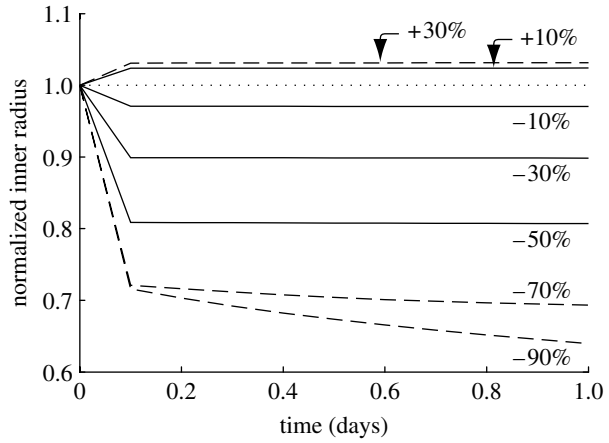


Figure 2. Numerically instantaneous (i.e. first computational time step) constrictions and dilations for a range of flow rates (shown as ±per cent changes from $Q_h$). Solid lines represent cases in which the instantaneous change in radius returns $\tau_w = \tau_w^h$. Dashed lines represent cases for which the vessel cannot accommodate the altered flow with a single instantaneous constriction or dilation. Dotted line represents the case for which $Q(s) = Q_h$. Note the bias towards constriction rather than dilation, which is consistent with the behaviour of cerebral arteries (Faraci 1990). Also note the clearly defined limit for maximal instantaneous constriction. One can see initial G&R governed changes for large reductions in flow rate (beyond what the vessel can accommodate instantaneously) as a gradual decrease in radius after the step change. A corresponding delayed increase in radius for the 30% increase in flow is not discernible at this short time scale. All parameters $K_\sigma^k = K_C^k = 1$.

Table 1. Parameter values used to simulate the response of a basilar artery that consists primarily of smooth muscle and collagen.

| |
|---|
| prestretches and elastic parameters |
| $G_h^e = 1.4$, $G_h^c = 1.08$, $G_h^m = 1.2$ |
| $c = 382.4$ kPa |
| $c_2^c = 22$, $c_2^m = 3.5$ |
| $c_1^c = 280.2$ kPa, $c_1^m = 36.5$ kPa |
| muscle activation parameters |
| $T_{max} = 150$ kPa |
| $\lambda_M = 1.1$, $\lambda_0 = 0.4$ |
| $C_B = 0.68$, $C_S = 20 C_B$ |
| initial mass fractions and half-lives |
| $\phi_0^c = 0.22$, $\phi_0^e = 0.02$, $\phi_0^m = 0.76$ |
| $K_h^m = 1/80$ day$^{-1}$, $K_h^c = 1/80$ day$^{-1}$ |

dilations beyond that limit must be governed exclusively by changes in stress (see equations (2.14) and (2.16)). Thus, delayed dilations occur much more slowly than delayed constrictions (figures 2 and 3) as a consequence of the inherent bias towards constrictors within our relations for mass density production and active muscle behaviour, consistent with NO-inhibiting and ET-1-promoting turnover. Indeed, increasing flow in adult rabbit carotids by 60 per cent results in no enlargement within two months and no changes in thickness or medial cross-sectional area (Brownlee & Langille 1991). This is consistent with our model's predictions, as inner radius restores wall shear stress only after at least 100 days following a substantial increase in flow.

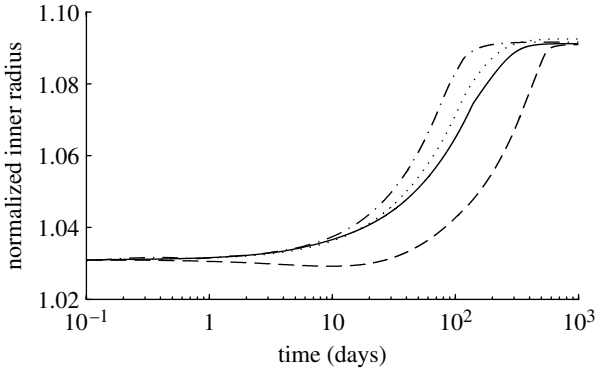


Figure 3. Normalized inner radius over 1000 days for 30% increases in flow where $K_\sigma^k = K_C^k = 1$ (dotted line), $K_\sigma^k = 1$ and $K_C^k = 10$ (dot-dashed line), $K_\sigma^k = 10$ and $K_C^k = 1$ (dashed line) and $K_\sigma^k = K_C^k = 10$ (solid line). Note the dramatically delayed dilation for the case in which $K_\sigma^k > K_C^k$. Note also that a 30% increase in flow should produce a 9% increase in calibre, which is predicted by the model.

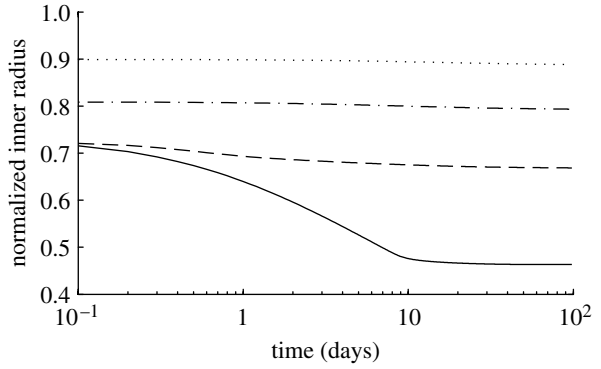


Figure 4. Normalized inner radius over 100 days for 30% (dotted line), 50% (dot-dashed line), 70% (dashed line) and 90% (solid line) reductions in flow. Note the instantaneous constrictions and the marked delayed changes for the case of a 90% reduction in flow. Note also that a 90% reduction in flow should produce a 54% decrease in calibre, which is predicted by the model. All parameters $K_\sigma^k = K_C^k = 1$.

As inner radius increases (or decreases) to return $\tau_w(s)$ towards its homeostatic target, the mean circumferential stress will initially increase (or decrease) due to the thinning (thickening) of the vessel wall from an isochoric motion. These changes in circumferential stress drive further, albeit perhaps more gradual, G&R, and wall thickness continues to change long after the step change in flow (figure 5). Because $\tau_w$ is nearly returned to its homeostatic value almost immediately, this manifestation of G&R occurs more slowly, being driven by changes in circumferential stress without the additive effect of changes in constrictor concentration (figures 6–8).

As the vessel constricts in response to reduced $\tau_w$, collagen fibres are unloaded, and the stresses borne by collagen are drastically reduced. This provides a negative input to the production function (see equation (2.16)); that is, it promotes atrophy. On the other hand, the increase in constrictors (figure 8) provides a positive input to the production rate. Depending on the values of $K_C^k$ and $K_\sigma^k$, this dynamic interplay can have drastically different consequences on the simulated morphology and overall wall composition (figure 7).

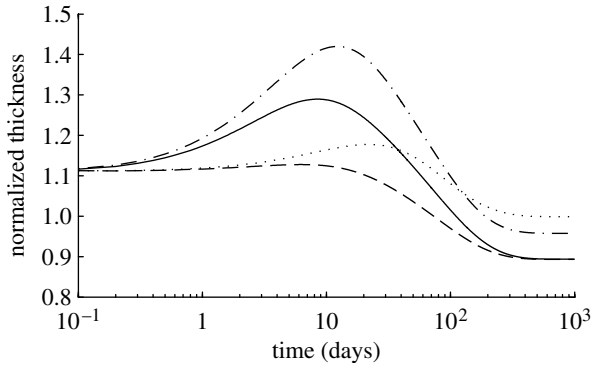


Figure 5. Normalized wall thickness over 1000 days for a 30% reduction in flow, where $K^k_\sigma = K^k_C = 1$ (dotted curve), $K^k_\sigma = 1$ and $K^k_C = 10$ (dot-dashed curve), $K^k_\sigma = 10$ and $K^k_C = 1$ (dashed curve) and $K^k_\sigma = K^k_C = 10$ (solid curve). The model predicts an initial thickening as the production rate of smooth muscle increases and causes accumulation (figures 6 and 7). After the first week, however, some collagen is degraded, and the wall begins to lose mass. In all cases, wall thickness is stable after approximately 500 days, although the expected value (88% of original) is only attained for cases where $K^k_\sigma > 1$.

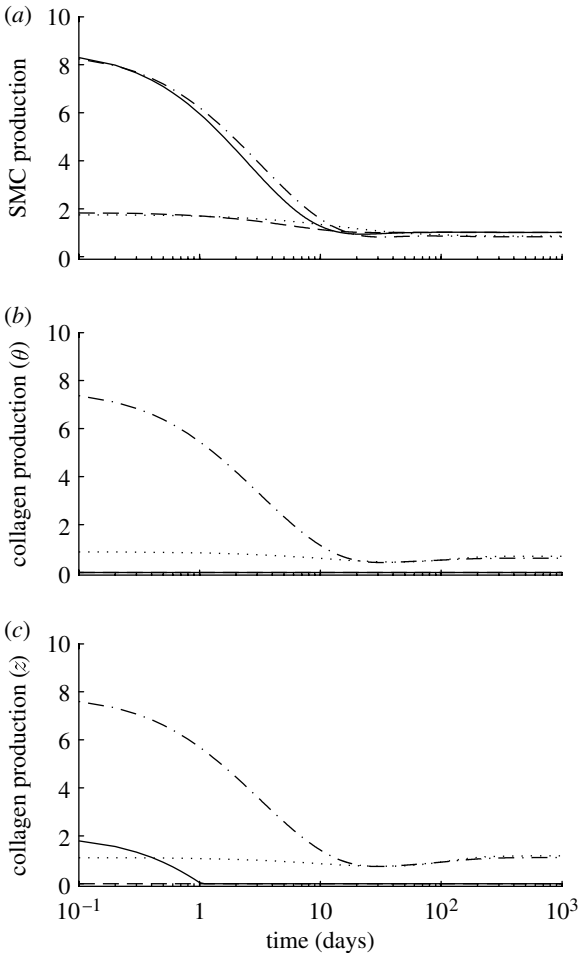


Figure 6. Time courses of mass density production rates, normalized with respect to homeostatic rates, for (*a*) smooth muscle, (*b*) circumferentially oriented collagen and (*c*) axially oriented collagen for a 30% reduction in flow, where $K^k_\sigma = K^k_C = 1$ (dotted line), $K^k_\sigma = 1$ and $K^k_C = 10$ (dot-dashed line), $K^k_\sigma = 10$ and $K^k_C = 1$ (dashed line) and $K^k_\sigma = K^k_C = 10$ (solid line). Note the rapid (unrealistic) drop in the rate of collagen production for the cases where $K^k_\sigma = 10$. Time courses for helical collagen (not shown) follow the same general trends as axial collagen. Note also that fold changes in production rates are within expected ranges (cf. Xu *et al.* 2000).

For instance, when $K^k_\sigma = 10$, the negative input from the unloaded collagen serves to effectively halt its production (figure 6*b*,*c*). Conversely, when $K^k_C \geq K^k_\sigma$, the production rates for collagen increase substantially as the increase in $C(s)$ overwhelms reductions due to stress-mediated mass production. Since smooth muscle can actively generate force, its production rate remains positive. In fact, because muscle is always actively constricting the vessel in cases of reduced flow, its production rates are always above the homeostatic value as both the stress and constrictor levels provide positive inputs into muscle production (figure 6*a*). Langille *et al.* (1989) reported no significant change in medial mass or constituent fraction ratios after one month of reduced flow in carotids. Our results predict little medial remodelling after 30 days (figure 7), consistent with this observation. Although they reported no significant changes in mass or wall constituents, they did report a markedly undulated appearance in internal elastic laminae. This is most likely a result of the unloading of elastin due to the reduced inner radius and is consistent with our hypothesis that elastin does not remodel in adults. Brownlee & Langille (1991) reported that after one week of reduced flow and a subsequent restoration of flow, the vessel reverted to its original calibre. This implicates different and as yet unknown mechanisms for remodelling in cases of increased flow (from normal) versus cases of decreased and subsequent restoration of normal flow. This may be related to the elastin not turning over and retaining its ability to return to its original length without exceeding its homeostatic stress. Our model predicts similar behaviour (figure 9).

Histological changes in collagen and muscle have measurable mechanical effects on the vessel. The simulated passive response to reduced blood flow involves an initial stiffening, due to a modest increase in muscle deposition, followed by a gradual increase in compliance as the vessel loses circumferential collagen (figure 7). After 1000 days, the vessel is predicted to be slightly more compliant than at day 0 (figure 10*a*), though this difference would be within experimental noise. In fact, this shift towards compliance is complete after 500 days (not shown) when all parameters $K^k_\sigma = K^k_C = 1$. For cases where $K^k_\sigma \geq K^k_C$, the vessel's eventual shift towards increased compliance is complete within 300 days (not shown), due to a (unrealistic) nearly complete loss of collagen. This difference in the time to converge on a stable passive mechanical behaviour highlights the importance of the parameters within equation (2.16) from the point of view of the time course of the vessel's evolution. Nonetheless, the model predicts a modest passive softening regardless of the values used therein.

Finally, figure 10*b* shows the evolving active behaviour as the vessel accommodates a 30 per cent reduction in flow. Note the rapid leftward shifting of the curve due to smooth muscle being turned over in the new vasoconstricted state. The maximum values for stress are related to evolving constrictor levels

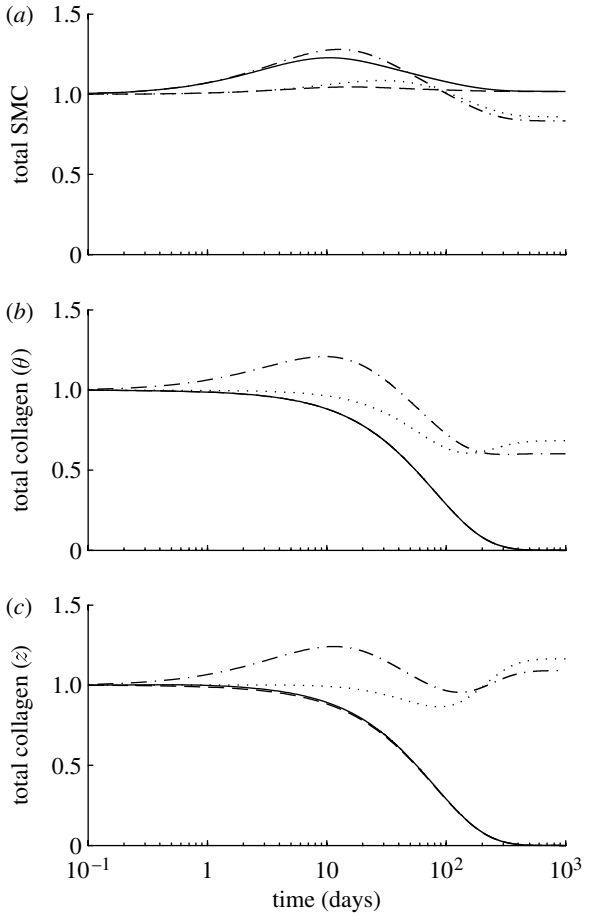


Figure 7. Time courses of changes in total mass, normalized with respect to homeostatic values, for (*a*) smooth muscle, (*b*) circumferentially oriented collagen and (*c*) axially oriented collagen for a 30% reduction in flow, where $K_\sigma^k = K_C^k = 1$ (dotted line), $K_\sigma^k = 1$ and $K_C^k = 10$ (dot-dashed line), $K_\sigma^k = 10$ and $K_C^k = 1$ (dashed line) and $K_\sigma^k = K_C^k = 10$ (solid line). Note the eventual (unrealistic) complete loss of collagen for the cases where $K_\sigma^k = 10$. The time courses for helical collagen (not shown) follow the same general trends as axial collagen.

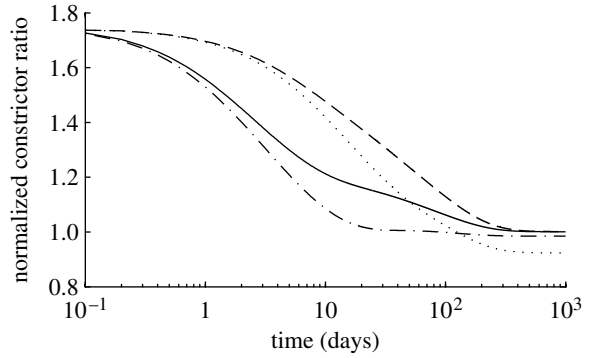


Figure 8. Time courses of constrictor concentration ratio $C(s)$, normalized with respect to $C_\mathrm{B}$, for a 30% reduction in flow where $K_\sigma^k = K_C^k = 1$ (dotted line), $K_\sigma^k = 1$ and $K_C^k = 10$ (dot-dashed line), $K_\sigma^k = 10$ and $K_C^k = 1$ (dashed line) and $K_\sigma^k = K_C^k = 10$ (solid line). Note the return to baseline, but at very different rates depending on the values for the production rate parameters. This emphasizes the complex coupling between endothelial function and wall biomechanics.

(see equation (2.14) and figure 8) as well as the evolving loaded active muscle length $a^{\mathrm{m(act)}}(s)$, with increasing constriction occurring in the first 7 days and gradual

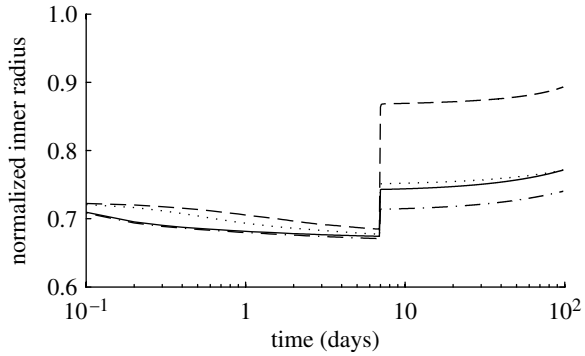


Figure 9. Normalized inner radius over 100 days for a 70% reduction in flow at day 0 and a restoration of blood flow at day 7, where $K_\sigma^k = K_C^k = 1$ (dotted line), $K_\sigma^k = 1$ and $K_C^k = 10$ (dot-dashed line), $K_\sigma^k = 10$ and $K_C^k = 1$ (dashed line) and $K_\sigma^k = K_C^k = 10$ (solid line).

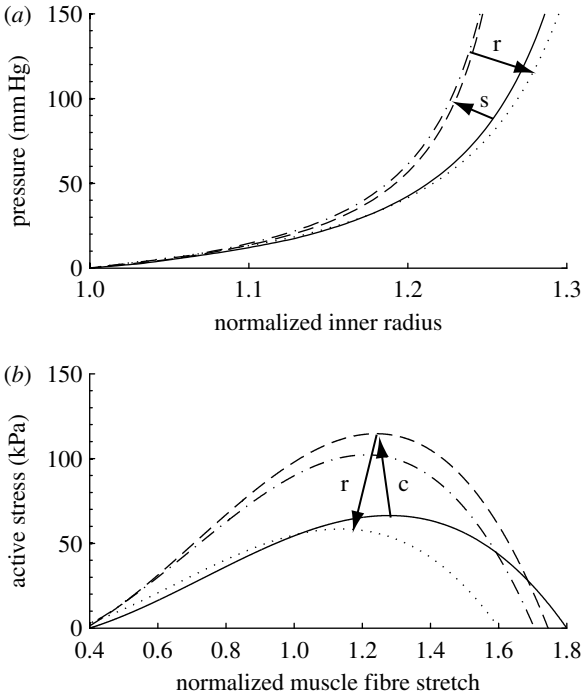


Figure 10. (*a*) Evolving passive 'pressure–diameter' curves at days 0 (solid curve), 7 (dashed curve), 14 (dot-dashed curve) and 1000 (dotted curve) for a 30% reduction in flow. All parameters $K_\sigma^k = K_C^k = 1$. The abscissa 'normalized inner radius' is expressed as the ratio of the current deformed inner radius to the current unloaded inner radius ($a(s)/A(s)$). The rapid initial shift to the left indicates stiffening (s) due to gradual turnover of constituents such as collagen and resultant thickening of the vessel wall in the vasoconstricted state. The gradual rightward shift indicates passive relaxation (r) while the vessel loses mass. Note that after 1000 days, the simulated vessel is slightly more compliant than at day 0, but this would be within experimental noise. (*b*) Predicted shifting of the active muscle response due to G&R at days 0 (solid curve), 7 (dashed curve), 14 (dot-dashed curve) and 1000 (dotted curve), also for a 30% decrease in flow. The abscissa 'normalized muscle fibre stretch' is expressed as a range of values for $\lambda_\theta^{\mathrm{m(act)}}(s)a^{\mathrm{m(act)}}(s)/a^{\mathrm{m(act)}}(0)$. Increasing constriction (c) occurs over the first 7 days followed by a gradual relaxation (r) as the constrictor levels return to normal.

relaxation occurring as the constrictor levels return to normal. Langille *et al.* (1989) observed an early reduction in radius associated with the vasoactive

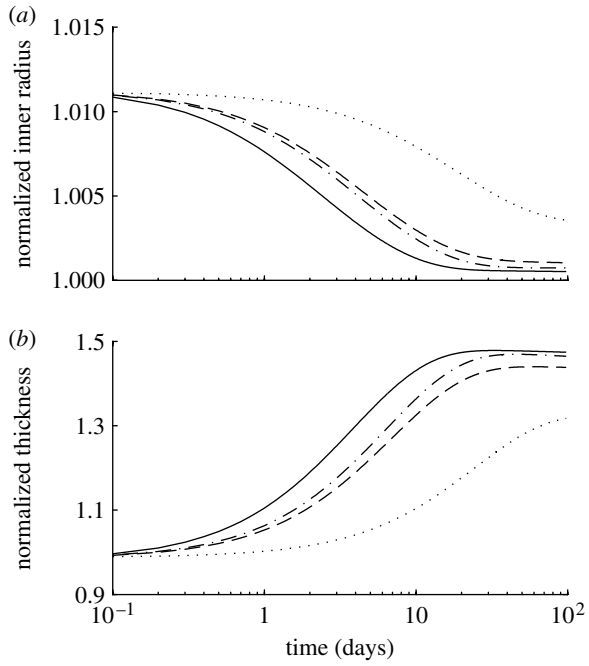


Figure 11. Geometric changes over 100 days in (*a*) normalized radius and (*b*) thickness in response to a 50% increase in pressure, where $K_\sigma^k = K_C^k = 1$ (dotted lines), $K_\sigma^k = 1$ and $K_C^k = 10$ (dot-dashed lines), $K_\sigma^k = 10$ and $K_C^k = 1$ (dashed lines) and $K_\sigma^k = K_C^k = 10$ (solid lines). The inner radius initially increases due to the passive response to an increase in pressure, but the vessel can largely recover its inner radius within two weeks in order to restore $\tau_{\mathrm{w}}^{\mathrm{h}}$. Wall thickness increases as collagen and smooth muscle are deposited in response to increased circumferential stresses. The vessel can also attain a stable wall thickness within two weeks.

response followed by entrenchment (two weeks), with the vessel essentially functioning as a smaller vessel after one month. After 3 days, papaverine (a vasodilator) was able to reverse the constriction, suggesting that little to no G&R entrenchment had taken place. After one week, papavarine was able to reverse only half of the constriction suggesting that modest smooth muscle G&R entrenchment had taken place, and after two weeks, papavarine was unable to reverse the constriction, suggesting full entrenchment. Similarly, Brownlee & Langille (1991) reported fully reversible dilation after 3 days of reduced flow but irreversible vasoactive entrenchment after one month. This progression suggests a full shift in contractile response by two weeks. Our model predicts comparable time courses (figure 10*b*). This progression can be observed morphologically since a large nuclear profile in smooth muscle cells (SMCs) indicates that SMCs have not yet returned to their normal lengths (Langille *et al.* 1989).

### *3.2. Altered pressure*

The most conspicuous consequence of hypertension in arteries is a thickening of the wall that tends to restore the circumferential stress towards its normal value (Wolinsky 1970; Matsumoto & Hayashi 1996; Fridez *et al.* 2002; Hu *et al.* 2007*a*,*b*). This is a more delayed manifestation of vascular adaptation compared with the instantaneous reduction in calibre observed in the case of reduced flow simply because the vessel must

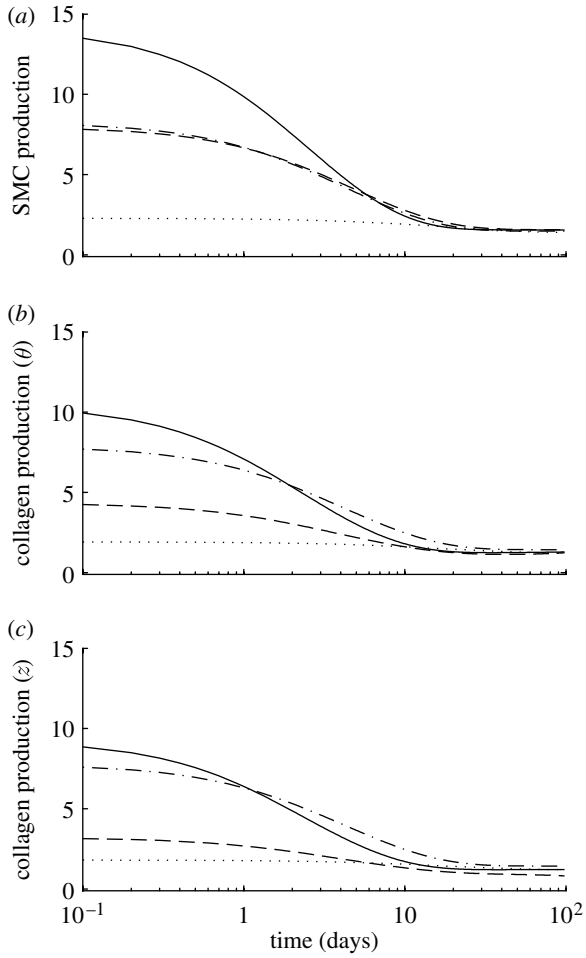


Figure 12. Time courses of mass density production rates, normalized with respect to the homeostatic rates, for (*a*) smooth muscle, (*b*) circumferentially oriented collagen and (*c*) axially oriented collagen for a 50% increase in pressure, where $K_\sigma^k = K_C^k = 1$ (dotted line), $K_\sigma^k = 1$ and $K_C^k = 10$ (dot-dashed line), $K_\sigma^k = 10$ and $K_C^k = 1$ (dashed line) and $K_\sigma^k = K_C^k = 10$ (solid line). Time courses for helical collagen (not shown) follow the same general trends as axial collagen.

accumulate mass over some period. In the case of an increase in transmural pressure, the vessel instantaneously distends due to the gross passive behaviour of the mixture (figure 11*a*). All constituents thus initially support greater loads, causing $\Delta\boldsymbol{\sigma}$ to increase. In addition, the increase in inner radius results in a decrease in $\tau_{\mathrm{w}}$ and an associated increase in $C(t)$. These effects work synergistically to increase mass production (figure 12), resulting in mass accumulation (figure 13) and wall thickening (figure 11*b*). Note the trend for the wall to thicken by nearly 50 per cent for a 50 per cent increase in pressure, which is consistent with expectations based on a simple force balance.

The predicted accumulation of collagen is qualitatively similar to observed morphological changes in basilar arteries (cf. fig. 6 in Hu *et al.* 2007*b*) and causes irreversible passive stiffening (figure 14*a*). Our model predicts stiffening within two weeks, with only modest subsequent stiffening to day 100. Similar behaviour has also been observed within two to four weeks in basilar arteries in animal models (Hu *et al.* 2007*a*,*b*). The model also predicts a negligible change in the active muscle length (figure 14*b*), as the inner diameter

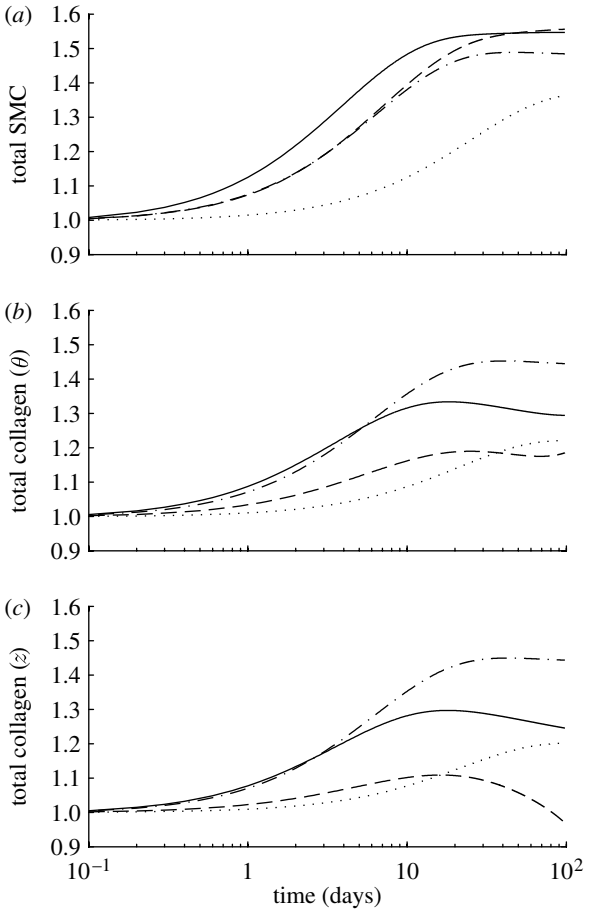


Figure 13. Time courses of total mass, normalized with respect to the homeostatic masses, for (*a*) smooth muscle, (*b*) circumferentially oriented collagen and (*c*) axially oriented collagen for a 50% increase in pressure, where $K_\sigma^k = K_C^k = 1$ (dotted line), $K_\sigma^k = 1$ and $K_C^k = 10$ (dot-dashed line), $K_\sigma^k = 10$ and $K_C^k = 1$ (dashed line) and $K_\sigma^k = K_C^k = 10$ (solid line). Note the accumulation of mass for almost all fibre families. The time courses for helical collagen (not shown) follow the same general trends as axial collagen.

changes only slightly, with maximum active stresses varying with $C(s)$ (figure 15). The values for $K_\sigma^k$ and $K_C^k$ again had large influences on the various predicted time courses. Clearly, production rates are directly proportional to these parameters; higher values result in accelerated changes in morphology and geometry.

The changes in unloaded length have been reported with decreasing longitudinal retractions in hypertensive canine aorta (Vaishnav *et al.* 1990). Our model predicts an increased unloaded length and inner radius with time (figure 16), which is qualitatively consistent with this observation. These changes are related to the quantities in axially and circumferentially oriented collagen, as collagen's smaller prestretch serves to restrict the retractive effects of elastin.

## 4. DISCUSSION

We have learned much about the biomechanics of the arterial wall over the past four decades (cf. Fung 1993; Humphrey 2002), yet we are just beginning to understand and quantify the remarkable ability of arteries to adapt in response to altered mechanical loading. For example, arteries increase in calibre in response to

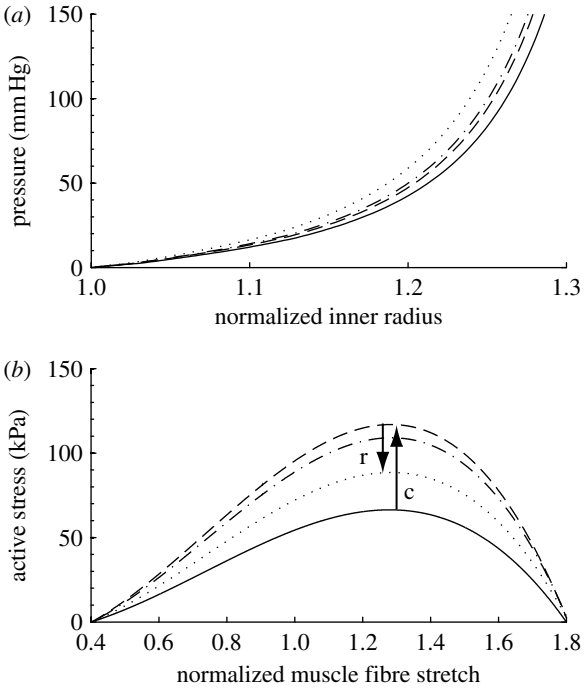


Figure 14. (*a*) Evolving passive 'pressure–diameter' curves at days 0 (solid curve), 7 (dashed curve), 14 (dot-dashed curve) and 100 (dotted curve) for a 50% increase in pressure. All parameters $K_\sigma^k = K_C^k = 1$. The abscissa 'normalized inner radius' is expressed as the ratio of the current deformed inner radius to the current unloaded inner radius ($a(s)/A(s)$). The irreversible shift to the left indicates stiffening due to gradual accumulation of constituents as the vessel wall thickens in response to increased circumferential stress. (*b*) Predicted shifting of active muscle response due to G&R at days 0 (solid curve), 7 (dashed curve), 14 (dot-dashed curve) and 100 (dotted curve), also for a 50% increase in pressure. The abscissa 'normalized muscle fibre stretch' is expressed as a range of values for $\lambda_\theta^{\mathrm{m(act)}}(s)a^{\mathrm{m(act)}}(s)/a^{\mathrm{m(act)}}(0)$. Note the very modest shifting of the curve, due to a correspondingly modest change in vessel radius. The maximum values for stress are related to evolving constrictor levels (see equation (2.14) and figure 15). The 'residual' elevation in active stress may reflect the lower NO production reported in hypertension and often referred to as 'endothelial dysfunction'.

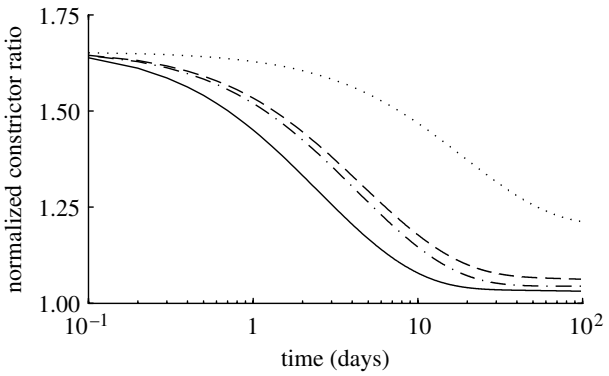


Figure 15. Time courses of constrictor concentration ratio $C(s)$, normalized with respect to $C_\mathrm{B}$, for a 50% increase in pressure, where $K_\sigma^k = K_C^k = 1$ (dotted line), $K_\sigma^k = 1$ and $K_C^k = 10$ (dot-dashed line), $K_\sigma^k = 10$ and $K_C^k = 1$ (dashed line) and $K_\sigma^k = K_C^k = 10$ (solid line). The early vasoconstriction offsets the initial increased elastic distension (Humphrey & Wilson 2003).

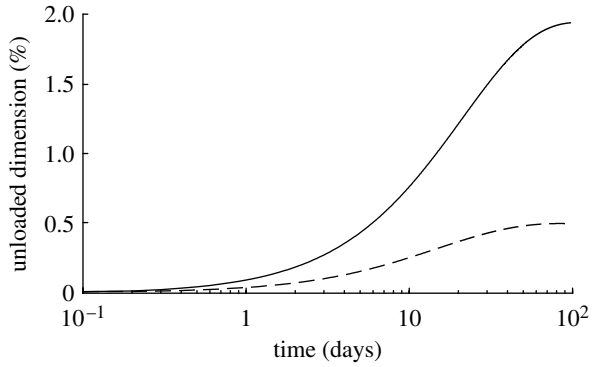


Figure 16. Time courses of per cent changes in unloaded axial length (solid line) and unloaded inner radius (dashed line) for a 50% increase in pressure. All parameters $K_\sigma^k = K_C^k = 1$.

increased flow, they thicken in response to increased pressure and they lengthen in response to increased axial loading (e.g. Wolinsky 1970; Kamiya & Togawa 1980; Langille *et al.* 1989; Matsumoto & Hayashi 1996; Jackson *et al.* 2002; Gleason *et al.* 2007).

It is instructive to consider simple geometric implications of stress-mediated G&R in response to altered flow and pressure (Humphrey 2008). Let homeostatic values be given by

$$\tau_{\mathrm{w}}^{\mathrm{h}} = \frac{4\mu Q_{\mathrm{h}}}{\pi a_{\mathrm{h}}^3}, \qquad \sigma_\theta^{\mathrm{h}} = \frac{P_{\mathrm{h}} a_{\mathrm{h}}}{h_{\mathrm{h}}}, \tag{4.1}$$

and consider a step change to new values of flow and pressure via $Q = \varepsilon Q_{\mathrm{h}}$ and $P = \gamma P_{\mathrm{h}}$. Hence, if both wall shear and circumferential stress are returned towards homeostatic values, then

$$\tau_{\mathrm{w}} = \frac{4\mu(\varepsilon Q_{\mathrm{h}})}{\pi a^3} \to \frac{4\mu Q_{\mathrm{h}}}{\pi a_{\mathrm{h}}^3}, \tag{4.2}$$

$$\sigma_\theta = \frac{\gamma P_{\mathrm{h}} a}{h} \to \frac{P_{\mathrm{h}} a_{\mathrm{h}}}{h_{\mathrm{h}}}, \tag{4.3}$$

or $a \to \varepsilon^{1/3} a_{\mathrm{h}}$ and $h \to \gamma(a/a_{\mathrm{h}}) h_{\mathrm{h}} = \gamma \varepsilon^{1/3} h_{\mathrm{h}}$. In other words, we see that the changes in flow affect both wall shear stress and circumferential stress, and thus both luminal radius and wall thickness, provided the vessel attempts to restore these stresses to normal. As seen in figures 2–5 and 11, the present simulations predict this trend, and, as noted in the figure captions, provide the correct degree of change (e.g. $a = (0.7)^{1/3} a_{\mathrm{h}} = 0.88 a_{\mathrm{h}}$ for a 30% reduction in flow).

Whereas these simple results suggest what should happen, the G&R framework addresses how these changes can occur. Our model predicts changes in geometry, structure and mechanical behaviour as natural consequences of biochemomechanically mediated G&R and the need to satisfy equilibrium at each G&R time. This is in contrast to other models that prescribe changes in geometry, properties and/or constituent mass fractions as functions of time or evolving stress differences (Taber 1998; Rachev 2000; Gleason *et al.* 2004; Tsamis & Stergiopulos 2007). Thus, our approach allows for a more realistic framework in which to model vascular G&R. Also, in contrast to previous work (e.g. Gleason *et al.* 2004), where the focus was on modelling geometric and morphological changes as functions of non-dimensional time, we have also extended the constrained mixture approach to occur continuously in actual time.

Although we focused on the basilar artery, we did not attempt to model any one experimental dataset from the literature (largely because no single study provides data sufficient for detailed modelling). Nevertheless, the current predictions represent a marked improvement over prior models in capturing salient features of flow- and pressure-induced adaptations in diverse arteries. Predictions show the importance of combined effects of altered vasoactivity and matrix turnover (cf. Fridez *et al.* 2002; Dajnowiec & Langille 2007), including potential differences between the initial extents of vasodilatation and vasoconstriction; they show that adaptations can occur faster in cases of decreased compared with increased flow (cf. Brownlee & Langille 1991); they show that wall shear stress can be restored to normal faster than intramural stress in cases of increased flow (cf. Masuda *et al.* 1999); they show that active length-tension behaviours can evolve but be restored at a different diameter due to adaptations (cf. Langille *et al.* 1989); and they show that inner radius remains constant while wall thickness increases and thus circumferential wall stress normalizes within a few weeks in cases of increased pressure (cf. Matsumoto & Hayashi 1994; Fridez *et al.* 2002, 2003; Hu *et al.* 2007*b*). Indeed, by yielding reasonable time courses, in days to weeks or months, the current predictions suggest that complete adaptations may take longer than studied in some animal models. For example, Kamiya & Togawa (1980) reported carotid adaptations to increased flows at six to eight months and suggested 'an incomplete regulatory response to this extreme stress', that is, to flows more than fourfold higher than normal. Rather than an 'inherent limitation of the adaptive capacity', it may well be that longer times would be needed to achieve a complete adaptation for such a large perturbation.

Notwithstanding the ability of the current model to capture many observed features of flow- and pressure-induced remodelling in an artery, it cannot do so with a single set of model parameters. Therefore, there remains a pressing need for better constitutive relations for G&R and the data upon which they must be based. In particular, there is a need for more data on the time courses of stress-mediated alterations in cell proliferation and apoptosis as well as the synthesis and degradation of extracellular matrix. That is, although we know that the expression of growth factors, cytokines and matrix metalloproteinases changes significantly during adaptations to altered haemodynamics (e.g. Mondy *et al.* 1997; Singh *et al.* 1998; Xu *et al.* 2000, 2001; Sluijter *et al.* 2004), much remains unknown with regard to specific molar changes and the degree to which these affect cell activity. There is similarly a need for quantitative relationships that describe the multi-functional effects of vasoactive molecules. For example, we know that NO promotes endothelial cell proliferation while inhibiting both smooth muscle proliferation and its synthesis of matrix (Rizvi & Myers 1997; Dooley *et al.* 2007), but we lack precise empirical correlations for the extent of such changes as a function of shear-induced changes in the concentration of NO. Similarly, we know that ET-1

promotes smooth muscle proliferation and its synthesis of matrix (Rizvi *et al.* 1996; Rodriguez-Vita *et al.* 2005), but we lack precise relations in terms of shear-induced changes in the concentrations of ET-1. There is also a need to quantify relative changes in cell and matrix turnover in response to altered shear versus intramural stress. For example, decreased flow downregulates NO and upregulates ET-1, both of which should increase intramural production rates. Yet, the associated decrease in radius and initial isochoric increase in thickness due to vasoconstriction at a constant pressure will decrease intramural stress and thereby should decrease intramural production rates. We must understand better how specific changes in vasoactive concentrations and degrees of wall stress collectively control rates of turnover.

Once additional biochemical information is available, we could employ full mixture equations for mass balance whereby the arterial wall can consist of $N$ distinct types of constituents, $n$ of which are structurally significant (e.g. elastin, fibrillar collagens, smooth muscle). Separate mass balance equations for the $N-n$ soluble (e.g. NO, ET-1, growth factors) constituents $i=1, 2, \ldots, N-n$ and the $n$ insoluble (structural) constituents $k=1, 2, \ldots, n$ can then be written as

$$\frac{\partial \rho^i}{\partial s} + \mathrm{div}(\rho^i \boldsymbol{v}^i) = \tilde{m}^i, \quad \frac{\partial \rho^k}{\partial s} + \mathrm{div}(\rho^k \boldsymbol{v}^k) = \tilde{m}^k. \quad (4.4)$$

Here, $\rho^\alpha$ ($\alpha = i$ or $k$) are constituent (apparent) mass densities; $\boldsymbol{v}^\alpha$ are velocities; and $\tilde{m}^\alpha$ are net mass density productions. Consistent with the above, we could consider quasi-static deformations whereby the velocity of the arterial wall $\boldsymbol{v}$ is negligible. If we then invoke usual assumptions for dilute solutes (e.g. Fick's law of diffusion), the first of these two mass balance relations reduces to the standard reaction–diffusion equation

$$\frac{\partial C^i}{\partial s} = R^i + D^i \nabla^2 C^i, \quad (4.5)$$

where $C^i$ is the molar density for constituent $i$ (Slattery 1981), which is obtained from the mass density via the molecular weight; $R^i$ are reactions related to the net productions/losses; and $D^i$ are diffusivities. The diffusion term is important in three-dimensional problems, but less so for two-dimensional analyses of the arterial wall. Regardless, one could then use individual values of $C^i$ in the appropriate mass density production and removal functions (cf. equations (2.16) and (2.17)). As noted, however, this will require significantly more information on the specific biological responses.

Finally, we emphasize that constitutive relations do not describe a material (or cell activity) *per se*; rather, they describe responses by a tissue or cell to particular stimuli under specific conditions of interest. It is thus unreasonable to expect that a single kinetic relation for mass density production or mass removal will model all responses of a vascular cell to all stimuli. With regard to the present discussion, we note that extreme increases in flow from normal could induce endothelial damage (Fry 1968) whereas extreme decreases in flow, including cessation of flow, could cause endothelial cells to upregulate adhesion molecules that capture circulating monocytes and promote local inflammatory processes or atherogenesis. Our current illustrative forms for mass density production and removal are not intended to capture such extremes. Likewise significant differences are expected during the progression from development to maturity and ageing; such differences were not addressed herein. For example, adaptations to increased blood flow are faster in younger compared with older animals (e.g. Brownlee & Langille 1991; Miyashiro *et al.* 1997), but we did not attempt to account for such differences. Indeed, there is a need to determine whether such differences are due primarily to higher basal turnover rates in younger animals (cf. Stenmark & Mecham 1997) or if the basic functional forms of the kinetic relations change with age. Finally, there is a need to delineate differences in response by elastic versus muscular arteries, intracranial versus extracranial and systemic versus pulmonary. Fortunately, it appears that the same fundamental hypotheses and theoretical framework hold for diverse vessels.

In summary, the present theoretical framework for arterial G&R and illustrative constitutive relations yield predictions similar to many observations reported in the literature. Nevertheless, there is a continued need for more data and better constitutive relations so that models can not only capture the consequences of G&R but also the mechanisms by which such changes occur. For purposes of illustration, we employed simple descriptions of wall mechanics and haemodynamics. Such simplicity can represent the situation in a straight cylindrical region such as the basilar artery, but more importantly, it is a prudent way to test basic concepts and to build intuition. One obvious advantage of this type of model is the ease with which various hypotheses can be proposed and tested. For example, results for a 30 per cent reduction in flow suggest that this model is very sensitive to values of $K_\sigma^k$ and $K_C^k$ (figures 6 and 7). This calls into question the relative roles of smooth muscle and collagen in cases of large reductions in flow. These results may motivate experiments to determine actual morphological changes, thus narrowing the range of values for the parameters used in this model. Nevertheless, given our growing understanding of modelling arterial mechanobiology and the associated G&R mechanics, there is a need to begin to move towards more complex situations wherein actual haemodynamics and wall mechanics can be solved together (see Humphrey & Taylor (2008) for a description of one such approach).

This work was supported, in part, by NIH grants HL-64372 and HL-80415.

## APPENDIX A

Rather than writing mass balance for constituent $k$ in terms of a net mass density production (which can be positive, negative or zero), it proves convenient to use the true mass density production (always non-negative) and an associated survival function. To appreciate this choice better, consider the special case wherein the true mass density production rate is constant up to time $s=0$, at which time an altered G&R stimulus changes

the production rate to a different constant value. Hence, let

$$\int_{-\infty}^{s} \frac{\partial M^k}{\partial \tau} \mathrm{d}\tau = \int_{-\infty}^{0} m^k(\tau) q^k(s,\tau) \mathrm{d}\tau + \int_{0}^{s} m^k(\tau) q^k(s,\tau) \mathrm{d}\tau, \tag{A 1}$$

$$\int_{-\infty}^{s} \frac{\partial M^k}{\partial \tau} \mathrm{d}\tau = m^k(s_0) \int_{-\infty}^{0} q^k(s,\tau) \mathrm{d}\tau + m^k(s_n) \int_{0}^{s} q^k(s,\tau) \mathrm{d}\tau. \tag{A 2}$$

Moreover, consider the *special case* wherein the survival function is given as a constant exponential decay, namely $q^k(s,\tau) = \mathrm{e}^{-K^k(s-\tau)}$, whereby our result becomes

$$\begin{aligned} M^k(s) &= m^k(s_0) \mathrm{e}^{-K^k s} \int_{-\infty}^{0} \mathrm{e}^{K^k \tau} \mathrm{d}\tau + m^k(s_n) \mathrm{e}^{-K^k s} \int_{0}^{s} \mathrm{e}^{K^k \tau} \mathrm{d}\tau \\ &= \frac{m^k(s_0)}{K^k} \mathrm{e}^{-K^k s} + \frac{m^k(s_n)}{K^k} \left(1 - \mathrm{e}^{-K^k s}\right). \end{aligned} \tag{A 3}$$

Evaluating this result at $s=0$ requires that $M^k(0) = m^k(s_0)/K^k$, thus placing a restriction on initial/homeostatic rates of production and decay. Note, too, that if the two production rates are the same (say $m_0^k$ as expected when there is no change in stimulus at $s=0$, as in tissue maintenance), then $M^k(s) = m_0^k/K^k$. Based on these results, it proves convenient to consider the more general form

$$M^k(s) = M^k(0)\, Q^k(s) + \int_{0}^{s} m^k(\tau) q^k(s,\tau) \mathrm{d}\tau, \tag{A 4}$$

whereby $Q^k(0) = 1$.

Next, consider the strain energy needed to model the elastic stress response. At $s=0$, equation (2.6) becomes

$$W^k(0) = \frac{M^k(0)\, Q^k(0)}{\rho} \widehat{W}^k\left(\boldsymbol{C}^k_{n(0)}\right) \equiv \phi^k(0) \widehat{W}^k\left(\boldsymbol{C}^k_{n(0)}\right), \tag{A 5}$$

or $\phi^k \widehat{W}^k$, which yields the classical rule of mixtures relation for the stresses. Alternatively, if the turnover occurs in an unchanging mechanical state (i.e. the natural configurations remain fixed and thus $n(\tau) = n(0)$), then

$$W^k(s) = \widehat{W}^k\left(\boldsymbol{C}^k_{n(0)}\right) \left( \frac{M^k(0)\, Q^k(s)}{\rho} + \int_{0}^{s} \frac{m^k(\tau)}{\rho} q^k(s,\tau) \mathrm{d}\tau \right), \tag{A 6}$$

which from the relation for mass density can be written as

$$W^k(s) = \widehat{W}^k\left(\boldsymbol{C}^k_{n(0)}\right) \left( \frac{M^k(s)}{\rho(s)} \right) \equiv \phi^k(s)\, W^k\left(\boldsymbol{C}^k_{n(0)}\right). \tag{A 7}$$

This, too, recovers a classical rule of mixtures relation for the stored energy as it should. Hence, we see that the proposed constitutive framework recovers basic special cases as it should.

## REFERENCES


Baek, S., Rajagopal, K. R. & Humphrey, J. D. 2006 A theoretical model of enlarging intracranial fusiform aneurysms. *J. Biomech. Eng.* **128**, 142–149. (doi:10.1115/1.2132374)

Baek, S., Valentín, A. & Humphrey, J. D. 2007 Biochemomechanics of cerebral vasospasm and its resolution: II. Constitutive relations and model simulations. *Ann. Biomed. Eng.* **35**, 1498–1509. (doi:10.1007/s10439-007-9322-x)

Brownlee, R. D. & Langille, B. L. 1991 Arterial adaptations to altered blood flow. *Can. J. Physiol. Pharmacol.* **69**, 978–983.

Dajnowiec, D. & Langille, B. L. 2007 Arterial adaptations to chronic changes in haemodynamic function: coupling vasomotor tone to structural remodelling. *Clin. Sci. (Lond.)* **113**, 15–23. (doi:10.1042/CS20060337)

Dooley, A., Gao, B., Shi-Wen, X., Abraham, D. J., Black, C. M., Jacobs, M. & Bruckdorfer, K. R. 2007 Effect of nitric oxide and peroxynitrite on type I collagen synthesis in normal and scleroderma dermal fibroblasts. *Free Radic. Biol. Med.* **43**, 253–264. (doi:10.1016/j.freeradbiomed.2007.04.017)

Dorrington, K. & McCrum, N. 1977 Elastin as a rubber. *Biopolymers* **16**, 1201–1222. (doi:10.1002/bip.1977.360160604)

Faraci, F. M. 1990 Role of nitric oxide in regulation of basilar artery tone *in vivo*. *Am. J. Physiol.* **259**(Pt 2), H1216–H1221.

Fridez, P., Makino, A., Kakoi, D., Miyazaki, H., Meister, J. J., Hayashi, K. & Stergiopulos, N. 2002 Adaptation of conduit artery vascular smooth muscle tone to induced hypertension. *Ann. Biomed. Eng.* **30**, 905–916. (doi:10.1114/1.1507326)

Fridez, P., Zulliger, M., Bobard, F., Montorzi, G., Miyazaki, H., Hayashi, K. & Stergiopulos, N. 2003 Geometrical, functional, and histomorphometric adaptation of rat carotid artery in induced hypertension. *J. Biomech.* **36**, 671–680. (doi:10.1016/S0021-9290(02)00445-1)

Fry, D. L. 1968 Acute vascular endothelial changes associated with increased blood velocity gradients. *Circ. Res.* **22**, 165–197.

Fung, Y. C. 1993 *Biomechanics: mechanical properties of living tissues*, 2nd edn. New York, NY: Springer.

Gleason, R. L. & Humphrey, J. D. 2004 A mixture model of arterial growth and remodeling in hypertension: altered muscle tone and tissue turnover. *J. Vasc. Res.* **41**, 352–363. (doi:10.1159/000080699)

Gleason, R. L. & Humphrey, J. D. 2005*a* Effects of a sustained extension on arterial growth and remodeling: a theoretical study. *J. Biomech.* **38**, 1255–1261. (doi:10.1016/j.jbiomech.2004.06.017)

Gleason, R. L. & Humphrey, J. D. 2005*b* A 2d constrained mixture model for arterial adaptations to large changes in flow, pressure and axial stretch. *Math. Med. Biol.* **22**, 347–369. (doi:10.1093/imammb/dqi014)

Gleason, R. L., Taber, L. A. & Humphrey, J. D. 2004 A 2-d model of flow-induced alterations in the geometry, structure, and properties of carotid arteries. *J. Biomech. Eng.* **126**, 371–381. (doi:10.1115/1.1762899)

Gleason, R. L., Wilson, E. & Humphrey, J. D. 2007 Biaxial biomechanical adaptations of mouse carotid arteries cultured at altered axial extension. *J. Biomech.* **40**, 766–776. (doi:10.1016/j.jbiomech.2006.03.018)

Holzapfel, G. A., Gasser, T. C. & Ogden, R. W. 2000 A new constitutive framework for arterial wall mechanics and a comparative study of material models. *J. Elast.* **61**, 1–48. (doi:10.1023/A:1010835316564)

Hu, J.-J., Baek, S. & Humphrey, J. D. 2007*a* Stress–strain behavior of the passive basilar artery in normotension and hypertension. *J. Biomech.* **40**, 2559–2563. (doi:10.1016/j.jbiomech.2006.11.007)

Hu, J.-J., Fossum, T. W., Miller, M. W., Xu, H., Liu, J.-C. & Humphrey, J. D. 2007*b* Biomechanics of the porcine basilar artery in hypertension. *Ann. Biomed. Eng.* **35**, 19–29. (doi:10.1007/s10439-006-9186-5)

Humphrey, J. D. 2002 *Cardiovascular solid mechanics: cells, tissues, and organs*. New York, NY: Springer.

Humphrey, J. D. 2008 Mechanisms of arterial remodeling in hypertension: coupled roles of wall shear and intramural stress. *Hypertension* **52**, 195–200. (doi:10.1161/HYPERTENSIONAHA.107.103440)

Humphrey, J. D. & Delange, S. L. 2004 *An introduction to biomechanics: solids and fluids, analysis and design*. New York, NY: Springer.

Humphrey, J. D. & Na, S. 2002 Elastodynamics and arterial wall stress. *Ann. Biomed. Eng.* **30**, 509–523. (doi:10.1114/1.1467676)

Humphrey, J. D. & Rajagopal, K. R. 2002 A constrained mixture model for growth and remodeling of soft tissues. *Math. Models Methods Appl. Sci.* **12**, 407–430. (doi:10.1142/S0218202502001714)

Humphrey, J. D. & Taylor, C. A. 2008 Intracranial and abdominal aortic aneurysms: similarities, differences, and need for a new class of computational models. *Annu. Rev. Biomed. Eng.* **10**, 221–246. (doi:10.1146/annurev.bioeng.10.061807.160439)

Humphrey, J. D. & Wilson, E. 2003 A potential role of smooth muscle tone in early hypertension: a theoretical study. *J. Biomech.* **36**, 1595–1601. (doi:10.1016/S0021-9290(03)00178-7)

Jackson, Z. S., Gotlieb, A. I. & Langille, B. L. 2002 Wall tissue remodeling regulates longitudinal tension in arteries. *Circ. Res.* **90**, 918–925. (doi:10.1161/01.RES.0000016481.87703.CC)

Kamiya, A. & Togawa, T. 1980 Adaptive regulation of wall shear stress to flow change in the canine carotid artery. *Am. J. Physiol.* **239**, H14–H21.

Langille, B. L. 1996 Arterial remodeling: relation to hemodynamics. *Can. J. Physiol. Pharmacol.* **74**, 834–841. (doi:10.1139/cjpp-74-7-834)

Langille, B. L. & O'Donnell, F. 1986 Reductions in arterial diameter produced by chronic decreases in blood flow are endothelium-dependent. *Science* **231**, 405–407. (doi:10.1126/science.3941904)

Langille, B. L., Bendeck, M. P. & Keeley, F. W. 1989 Adaptations of carotid arteries of young and mature rabbits to reduced carotid blood flow. *Am. J. Physiol.* **256**(Pt 2), H931–H939.

Lehman, R. M., Owens, G. K., Kassell, N. F. & Hongo, K. 1991 Mechanism of enlargement of major cerebral collateral arteries in rabbits. *Stroke* **22**, 499–504.

Malek, A. & Izumo, S. 1992 Physiological fluid shear stress causes downregulation of endothelin-1 mRNA in bovine aortic endothelium. *Am. J. Physiol.* **263**(Pt 1), C389–C396.

Masuda, H., Zhuang, Y. J., Singh, T. M., Kawamura, K., Murakami, M., Zarins, C. K. & Glagov, S. 1999 Adaptive remodeling of internal elastic lamina and endothelial lining during flow-induced arterial enlargement. *Arterioscler. Thromb. Vasc. Biol.* **19**, 2298–2307.

Matsumoto, T. & Hayashi, K. 1994 Mechanical and dimensional adaptation of rat aorta to hypertension. *J. Biomech. Eng.* **116**, 278–283. (doi:10.1115/1.2895731)

Matsumoto, T. & Hayashi, K. 1996 Stress and strain distribution in hypertensive and normotensive rat aorta considering residual strain. *J. Biomech. Eng.* **118**, 62–73. (doi:10.1115/1.2795947)

Miyashiro, J. K., Poppa, V. & Berk, B. C. 1997 Flow-induced vascular remodeling in the rat carotid artery diminishes with age. *Circ. Res.* **81**, 311–319.

Mondy, J. S., Lindner, V., Miyashiro, J. K., Berk, B. C., Dean, R. H. & Geary, R. L. 1997 Platelet-derived growth factor ligand and receptor expression in response to altered blood flow *in vivo*. *Circ. Res.* **81**, 320–327.

Murray, C. D. 1926 The physiological principle of minimum work: I. The vascular system and the cost of blood volume. *Proc. Natl Acad. Sci. USA* **12**, 207–214. (doi:10.1073/pnas.12.3.207)

Rachev, A. 2000 A model of arterial adaptation to alterations in blood flow. *J. Elast.* **61**, 83–111. (doi:10.1023/A:1010800703478)

Rachev, A. & Hayashi, K. 1999 Theoretical study of the effects of vascular smooth muscle contraction on strain and stress distributions in arteries. *Ann. Biomed. Eng.* **27**, 459–468. (doi:10.1114/1.191)

Rizvi, M. A. D. & Myers, P. R. 1997 Nitric oxide modulates basal and endothelin-induced coronary artery vascular smooth muscle cell proliferation and collagen levels. *J. Mol. Cell Cardiol.* **29**, 1779 –1789. (doi:10.1006/jmcc.1996.0480)

Rizvi, M. A. D., Katwa, L., Spadone, D. P. & Myers, P. R. 1996 The effects of endothelin-1 on collagen type I and type III synthesis in cultured porcine coronary artery vascular smooth muscle cells. *J. Mol. Cell Cardiol.* **28**, 243–252. (doi:10.1006/jmcc.1996.0023)

Rodbard, S. 1975 Vascular caliber. *Cardiology* **60**, 4–49.

Rodriguez-Vita, J., Ruiz-Ortega, M., Ruperez, M., Esteban, V., Sanchez-Lopez, E., Plaza, J. J. & Egido, J. 2005 Endothelin-1, via ETA receptor and independently of transforming growth factor-β, increases the connective tissue growth factor in vascular smooth muscle cells. *Circ. Res.* **97**, 125–134. (doi:10.1161/01.RES.0000174614.74469.83)

Rudic, R. D., Shesely, E. G., Maeda, N., Smithies, O., Segal, S. S. & Sessa, W. C. 1998 Direct evidence for the importance of endothelium-derived nitric oxide in vascular remodeling. *J. Clin. Invest.* **101**, 731–736. (doi:10.1172/JCI1699)

Singh, T. M., Abe, K. Y., Sasaki, T., Zhuang, Y. J., Masuda, H. & Zarins, C. K. 1998 Basic fibroblast growth factor expression precedes flow-induced arterial enlargement. *J. Surg. Res.* **77**, 165–173. (doi:10.1006/jsre.1998.5376)

Slattery, J. C. 1981 *Momentum, energy, and mass transfer in continua*. New York, NY: Krieger.

Sluijter, J. P. G., Smeets, M. B., Velema, E., Pasterkamp, G. & de Kleijn, D. P. V. 2004 Increase in collagen turnover but not in collagen fiber content is associated with flow-induced arterial remodeling. *J. Vasc. Res.* **41**, 546–555. (doi:10.1159/000081972)

Stenmark, K. R. & Mecham, R. P. 1997 Cellular and molecular mechanisms of pulmonary vascular remodeling. *Annu. Rev. Physiol.* **59**, 89–144. (doi:10.1146/annurev.physiol.59.1.89)

Taber, L. A. 1998 A model for aortic growth based on fluid shear and fiber stresses. *J. Biomech. Eng.* **120**, 348–354. (doi:10.1115/1.2798001)

Tsamis, A. & Stergiopulos, N. 2007 Arterial remodeling in response to hypertension using a constituent-based model. *Am. J. Physiol. Heart Circ. Physiol.* **293**, H3130–H3139. (doi:10.1152/ajpheart.00684.2007)

Uematsu, M., Ohara, Y., Navas, J. P., Nishida, K., Murphy, T. J., Alexander, R. W., Nerem, R. M. & Harrison, D. G.

1995 Regulation of endothelial cell nitric oxide synthase mRNA expression by shear stress. *Am. J. Physiol.* **269**(Pt 1), C1371–C1378.

Vaishnav, R. N., Vossoughi, J., Patel, D. J., Cothran, L. N., Coleman, B. R. & Ison-Franklin, E. L. 1990 Effect of hypertension on elasticity and geometry of aortic tissue from dogs. *J. Biomech. Eng.* **112**, 70–74. (doi:10.1115/1.2891128)

Wicker, B. K., Hutchens, H. P., Wu, Q., Yeh, A. T. & Humphrey, J. D. 2008 Normal basilar artery structure and biaxial mechanical behaviour. *Comput. Methods Biomech. Biomed. Eng.* **11**, 539–551. (doi:10.1080/10255840801949793)

Wolinsky, H. 1970 Response of the rat aortic media to hypertension. Morphological and chemical studies. *Circ. Res.* **26**, 507–522.

Xu, C., Zarins, C. K., Bassiouny, H. S., Briggs, W. H., Reardon, C. & Glagov, S. 2000 Differential transmural distribution of gene expression for collagen types I and III proximal to aortic coarctation in the rabbit. *J. Vasc. Res.* **37**, 70–82. (doi:10.1159/000025728)

Xu, C., Lee, S., Singh, T. M., Sho, E., Li, X., Sho, M., Masuda, H. & Zarins, C. K. 2001 Molecular mechanisms of aortic wall remodeling in response to hypertension. *J. Vasc. Surg.* **33**, 570–578. (doi:10.1067/mva.2001.112231)

Zamir, M. 1977 Shear forces and blood vessel radii in the cardiovascular system. *J. Gen. Physiol.* **69**, 449–461. (doi:10.1085/jgp.69.4.449)

Zarins, C. K., Zatina, M. A., Giddens, D. P., Ku, D. N. & Glagov, S. 1987 Shear stress regulation of artery lumen diameter in experimental atherogenesis. *J. Vasc. Surg.* **5**, 413–420. (doi:10.1067/mva.1987.avs0050413)